Analytical and Bioanalytical Chemistry
https://doi.org/10.1007/s00216-020-02860-w

RESEARCH PAPER

An electrochemical biosensor based on multi-wall carbon nanotube–modified screen-printed electrode immobilized by uricase for the detection of salivary uric acid

Weishan Shi[1] · Jing Li[1] · Jie Wu[1] · Qianying Wei[1] · Cuili Chen[1] · Ning Bao[1] · Chunmei Yu[1] · Haiying Gu[1]

Received: 8 July 2020 / Revised: 28 July 2020 / Accepted: 3 August 2020

Abstract

The amounts of uric acid (UA) in non-invasive biological samples, such as saliva, are critical for diagnosis and therapy of gout, hyperuricemia, Lesch–Nyhan syndrome, and several other diseases. Here, disposable UA biosensors were fabricated with the screen printing technique on the substrate of flexible PET. The working electrode was modified with carbon nanotubes followed by uricase for UA detection with excellent selectivity. The biosensor showed good electrocatalytic activity toward UA with high sensitivity, low detection limit, and wide linear range, which covers the full range of UA levels in human saliva. We demonstrate that UA can be directly detected in human saliva with the biosensor and the experimental data were consistent with the clinical analysis. This study indicated that the non-invasive biosensor is an attractive and possible approach for the monitoring of salivary UA.

Keywords Carbon nanotubes · Uric acid · Human saliva · Biosensor · Chronoamperometry

Introduction

Uric acid (UA) is a main end product of purine metabolism in the human body. The normal UA concentration in blood for healthy individuals varies between 100 and 400 μM [1]. The elevated UA level is related to many clinical disorders, such as gout, hyperuricemia, and Lesch–Nyhan syndrome [2, 3]. Additionally, other clinical studies have proved that the high UA level is also a risk for diabetes, kidney disease, and heart disease [4, 5]. Thus, determination of UA in human physiological fluids is important for diagnosis and treatment of these diseases.

In clinical practice, a common approach for UA testing requires the collection of blood samples, which is an invasive method and will cause unwillingness and resistance from patients. Previous reports suggested that there is a high correlation between salivary and serum UA levels [6], suggesting that non-invasive saliva may be a useful biological sample for probing UA. More importantly, the collection of saliva is painless and very simple, which is believed to be beneficial for clinical treatment. Therefore, determination of UA in saliva seems to be an attractive alternative for UA monitoring in clinical applications.

Conventionally, the clinical methods for the UA detection were based on spectrophotometry [7], fluorimetry [8], gas chromatography [9], and high-performance liquid chromatography [10]. However, most of those techniques are complex, time consuming, and requiring expensive equipment so that they are not suitable for daily personal use. Electrochemical method has been demonstrated to be an effective approach for rapid quantification in physiological analysis owing to the advantages, such as short detection time, low cost, and requirement of less amount of sample. Recently, several investigations have been carried out on electrochemical detection of UA [11–14]. However, development of inexpensive electrochemical biosensors for UA detection with high sensitivity and selectivity is still at progress. In addition, too few studies have focused on analysis of UA in authentic human saliva.

The development of disposable sensors has been of great significance in UA measurement for point-of-care testing [15]. Screen-printed sensors represent a vital analytical tool

✉ Chunmei Yu
cmyu@ntu.edu.cn

✉ Haiying Gu
hygu@ntu.edu.cn

[1] School of Public Health, Nantong University, Nantong 226019, Jiangsu, China

Published online: 13 August 2020

that fulfills the growing demand for miniaturization and sensitivity in biological analysis [16–20]. Reduction of analyte volume makes such approach attractive over conventional electrodes. In addition, the integration of nanomaterials on the electrode surface could increase the rates of electron transfer so as to improve the analytical performance of these sensors.

In this work, we describe a biosensor based on carbon nanotubes and uricase for detection of salivary UA in human saliva. The biosensor was developed with the screen printing technique on a flexible polyethyleneterephthalate (PET) substrate followed by modification of carbon nanotubes and uricase. The high aspect ratio and tensile strength allow the formation of flexible and conductive networks that can be used as flexible electrodes [21–23]. The disposable biosensor exhibits excellent amperometric response to UA with high sensitivity and selectivity. We demonstrated that the biosensor can be applied for directly monitoring of salivary UA in healthy volunteers and hyperuricemia patients. The effect of concentration of carbon nanotubes, loading of uricase for the electrode modification, and the potential on the performance of the biosensor was also investigated.

Experimental

Reagents and apparatus

Ag/AgCl conductive ink and carbon conductive ink were received from Shanghai Shuxing Technology Materials Co., Ltd. (Shanghai, China). Uricase (86 U/mg) was obtained from Shanghai Yuanye Biotechnology Co., Ltd. (Shanghai, China). Uric acid (UA), ascorbic acid (AA), dopamine (DA), NaCl, $CaCl_2$, KCl, citric acid, KSCN, and NH_4Cl were purchased from Aladdin Industrial Co., Ltd. (Shanghai, China) and used without further purification. Multi-walled carbon nanotubes (MWCNTs) (2 wt%) were obtained from Nanjing XFNANO Materials Technology Co., Ltd. (Nanjing, China). Polyethyleneterephthalate (PET) with 0.1 mm thick was purchased from China Lucky Group Co., Ltd. (Hefei, China). Phosphate buffer (PBS, 0.1 M) with various pH values was prepared from Na_2HPO_4 and NaH_2PO_4. To obtain the stock solution of UA, the solid UA was dissolved in 0.1 M NaOH firstly and then diluted with PBS to different concentrations. The artificial saliva was prepared by mixing 5 mM of NaCl, 1 mM of $CaCl_2$, 15 mM of KCl, 1 mM of citric acid, 1.1 mM of KSCN, and 4 mM of NH_4Cl. Deionized water was used during the entire experiments.

Electrochemical experiments were carried out on the CHI1230E electrochemical workstation (CH instrumentation, Shanghai, China). Scanning electron microscope (SEM) images were obtained from a Gemini SEM 300 scanning electron microscope (ZEISS, Germany). Solution of 0.1 M KNO_3 containing 5 mM $K_3[Fe(CN)_6]/K_4[Fe(CN)_6]$ (1:1) mixture was used for the electrochemical impedance spectroscopy (EIS) measurement. The chronoamperometric measurements were performed under a constant potential of 0.4 V (vs. Ag/AgCl) for 60 s after 1 min of incubation in the sample solution.

Design and fabrication of the biosensor

Home-made screen-printed electrodes (SPEs) used in this work are produced by screen printing method on flexible PET substrate. The patterns of the sensor were designed in AutoCAD and outsourced for manufacture on the framed stencils. Scheme 1 shows the fabrication process of the biosensor. PET was ultrasonically cleaned sequentially with acetone, ethanol, and deionized water for 5 min, respectively. Screen-printed three-electrode system was produced by sequential deposition of different commercial inks. First, the Ag/AgCl conductive ink was printed on the PET substrate to obtain the reference electrode and the connecting pad. Subsequently, conductive carbon ink was deposited on the PET to obtain the working and counter electrodes. The printed layers were cured at 70 °C for 10 min after every printing step. The working electrode is in a circle shape with a 3 mm diameter. The working electrode was subsequently modified with MWCNTs and uricase. Briefly, 1.0 mL of MWCNTs (2 wt%) was diluted with 1.0 mL of deionized water and sonicated for 1 h. Then, 3 μL of the obtained MWCNT suspension (1 wt%) was dropped on the working electrode and naturally dried. Next, an aqueous solution of uricase (3 μL from 1 mg/mL stock in 0.1 M pH 7.0 PBS) was drop-casted on the working electrode and incubated at 4 °C for 2 h. The obtained biosensor was denoted as uricase/MWCNTs/SPE. Uricase/SPE was fabricated according to the similar procedures in the absence of MWCNTs. The fabricated biosensors were tested in ferricyanide system to ensure the reproducibility and the stability of the biosensors.

Determination of UA in human saliva

Human saliva samples were collected from healthy volunteers and hyperuricemia patients (gifted from the Affiliated Hospital of Nantong University, China) using the "passive drooling" method [24]. The collection of samples was approved by the Ethics Committee of the Affiliated Hospital of Nantong University, and the experiments on human biologic samples were approved by the Ethics Committee of Nantong University. Before the collection of the samples, the participants were required to read and sign the consents as well as rinse the mouth thoroughly with deionized water.

The UA level in the human saliva samples was evaluated by the standard addition method. Briefly, 100 μL of saliva sample was firstly dropped on the electrode region. After 1 min of incubation, a constant potential of 0.4 V was applied

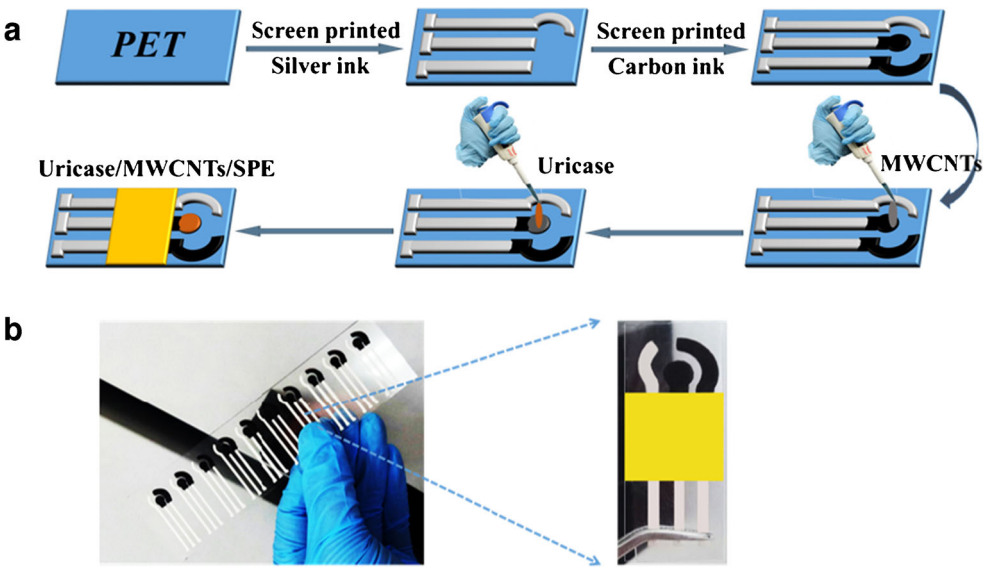

Scheme 1 **a** Schematic diagram of stepwise fabrication of the biosensor. **b** Photographs of the printed sensors

for 60 s to obtain the sample baseline. Subsequently, the saliva sample was spiked with the UA standard solution with different concentrations for current measurement under the same experimental conditions. The concentration of UA in saliva sample was evaluated based on the intercept of the calibration plot when the current is zero.

Results and discussion

Characterization of the biosensor

SEM was used to characterize the surface morphology of the biosensor. From Fig. 1a, we can see that the screen-printed carbon paste on the PET is quite rough at the micrometer scale and some carbon sheets overlap each other. In the magnified image, a lot of randomly distributed carbon particles attached to the entire electrode surface can be observed (Fig. 1b). The SEM image of MWCNTs/SPE shows that the MWCNTs are well distributed on the electrode surface, and most of the MWCNTs are in the form of small bundles (Fig. 1c). The porous net structure can not only increase the available surface area but also offer an excellent ability of electron transfer between the electrode and the analyte. After incubation of uricase on the biosensor, it was found that most of the MWCNTs are covered by the enzyme and the electrode surface becomes much smoother (Fig. 1d).

Cyclic voltammetry (CV) in the ferricyanide system is an effect tool for investigating the kinetic barrier of the interface. Figure 2A displays CVs of differently modified electrodes in a 5 mM ferricyanide solution. In the case of SPE, the peak-to-peak separation (ΔE_p) generated by the redox probe is

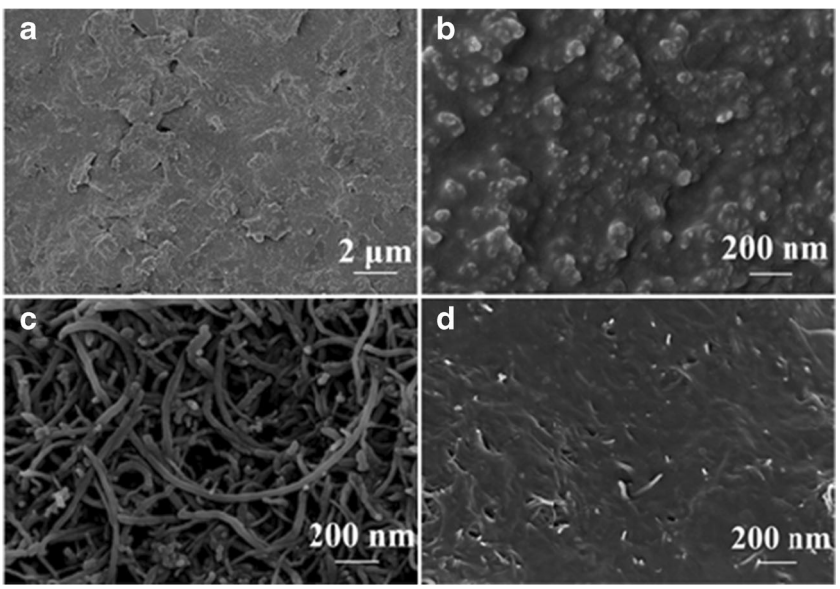

Fig. 1 SEM images of **a**, **b** SPE, **c** MWCNTs/SPE, and **d** uricase/MWCNTs/SPE

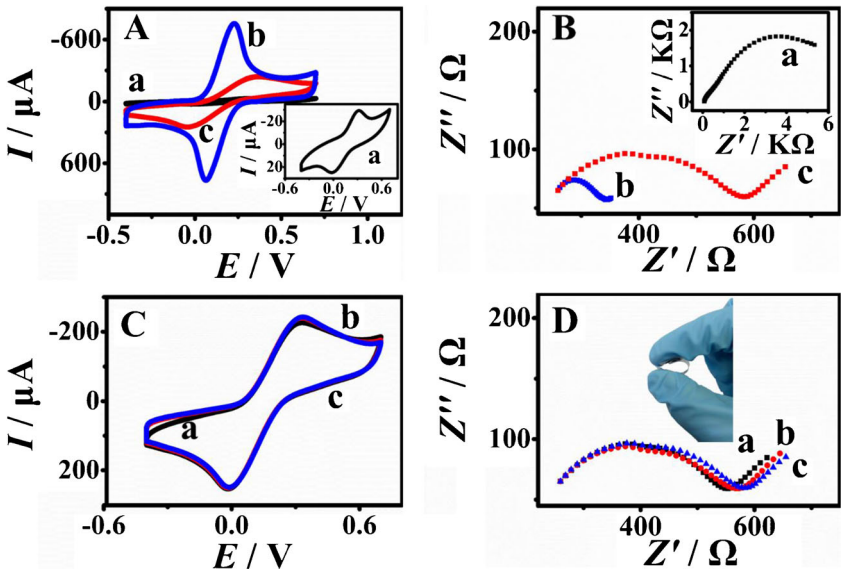

Fig. 2 **A** CVs and **B** EIS of (a) SPE, (b) MWCNTs/SPE, and (c) uricase/MWCNTs/SPE in 5 mM ferricyanide. Inset in **A**: the magnification of curve a. **C** CVs and **D** EIS of 5 mM ferricyanide recorded before and after applying 50 and 100 iterative bends for the uricase/MWCNTs/SPE

340 mV (inset). When the surface of the SPE was covered with MWCNTs, an obvious increase in the redox peak current and decrease in the ΔE_p (160 mV) are observed. The I_p of the MWCNTs/SPE is calculated as 52 times that of the bare SPE, indicating that MWCNTs can significantly increase the active surface area of the electrode and decrease the electron transfer distance between the redox probe and the underlying electrode. When uricase was incubated on the MWCNTs/SPE, an obvious reduction of the redox peak current and increase of the ΔE_p are observed, suggesting that the non-conductive uricase binding to the electrode surface would act as barriers which made the interfacial charge transfer inaccessible.

The impedance behaviors of the biosensor during the fabrication process were also studied (Fig. 2B). The SPE displays a large semicircle, suggesting a very high electron transfer resistance. The subsequent formation of MWCNT film results in a significant decrease of R_{ct}, implying that MWCNTs with good electrical conductivity could accelerate the electron transfer of the electrochemical probe. After the immobilization of uricase, the enzyme generates an insulating layer that in some degree blocks the probe, which is clearly indicated by the obvious increase of R_{ct}. The EIS results are in good agreement with the CV studies.

PET is a low-cost polymeric material which is flexible and reliable enough as sensor substrates for flexible devices [25–27]. Here, the fabricated biosensor also displayed the good flexibility. After 50 and 100 bending cycles, almost the same CVs are observed, indicating the bending had no effect on the structure and electrochemical performance of the biosensor (Fig. 2C). In addition, the EIS tests of the PET-based biosensor are almost completely coincident during the bending process (Fig. 2D). The results revealed that the high tensile strength of MWCNTs combined with flexible PET substrate results in the good mechanical flexibility of the biosensor, which is very beneficial for the storage and usage of the biosensor.

Electrochemical behavior of UA at the biosensor

Differential pulse voltammetry (DPV) was used to study the electrochemical behavior of UA at the biosensor with and without MWCNTs. When UA was absent in pH 7.0 PBS, there is no electrocatalytic oxidation peak at both the uricase/SPE and uricase/MWCNTs/SPE (curve a in Fig. 3A and B). After 100 μM UA was added, a broad oxidation peak at 0.31 V and a faint current signal are appeared at the uricase/SPE (curve b in Fig. 3A). The small current value indicates a low response sensitivity of the electrode. In contrast, significant enhancement of the response signal along with a more negative peak potential at about 0.16 V is achieved at the uricase/MWCNTs/SPE (curve b in Fig. 3B). The oxidation peak current at uricase/MWCNTs/SPE shows 26 times higher than that of uricase/SPE. It suggested that MWCNTs provide more spatial freedom for the uricase attached on the electrode surface, which will facilitate the electrocatalytic reaction of UA mediated with enzyme at the biosensor.

Figure 3C displays DPV curves of uricase/MWCNTs/SPE toward the continuous additions of UA in pH 7.0 PBS. It can be seen that the current response increases linearly with increasing the concentrations of UA in a wide concentration range, suggesting that the biosensor can be applied to detect UA with high sensitivity. In addition, chronoamperometry was also used to investigate the performance of the biosensors. As shown in Fig. 3D and E, the response signal for 100 μM UA at the uricase/SPE is much lower than that at the uricase/MWCNTs/SPE. The increase of UA concentration results in

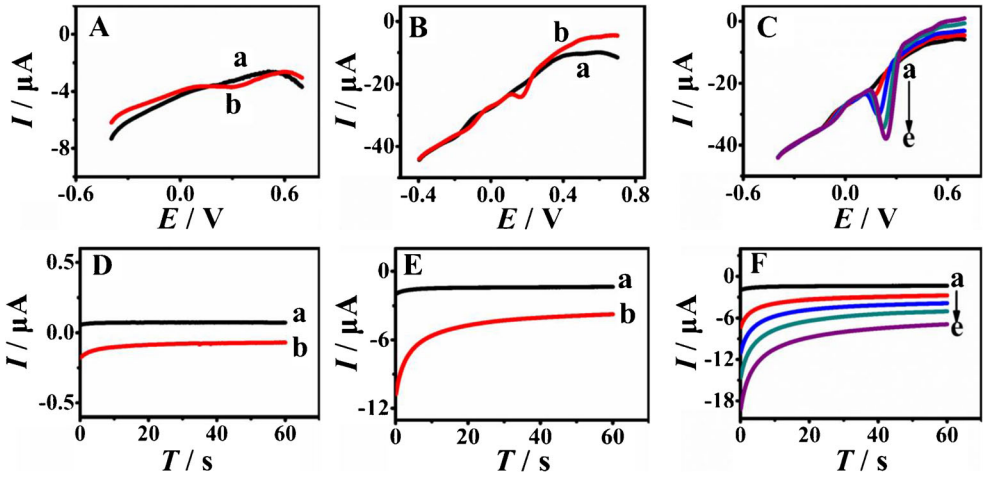

Fig. 3 DPVs of **A** uricase/MWCNTs/SPE and **B** uricase/SPE in the presence of (a) 0 and (b) 100 μM UA. **C** DPVs of uricase/MWCNTs/SPE upon the addition of different concentrations of UA (a–e: 0, 100, 300, 500, and 800 μM). Chronoamperograms of **D** uricase/MWCNTs/SPE and **E** uricase/SPE in the presence of (a) 0 and (b) 100 μM UA. **F** Chronoamperograms of the uricase/MWCNTs/SPE upon the addition of different concentrations of UA (a–e: 0, 100, 300, 500, and 800 μM)

the increasing current signal linearly, which is in accordance with the results of DPV (Fig. 3F). The remarkable improvement in the electrochemical performance of the MWCNT-based biosensor may be attributed to the fact that the MWCNTs can enlarge the surface area of the electrode and offer excellent electrical conductivity as well as catalytic performance for the UA analysis [28].

Optimization of experimental conditions

The concentrations of MWCNTs and uricase that immobilized on the electrode as well as the applied potential used in the chronoamperometric measurements would directly affect the sensitivity of the biosensor. To obtain the optimum performance, we investigated the response of 100 μM UA at the biosensor under different experimental conditions by chronoamperometry.

First, the effect of the concentration of MWCNTs on the performance of the biosensor was studied. As can be found from Fig. 4a, the current signal for 100 μM UA increases significantly when the concentration of MWCNTs increases from 0.2 to 1.0 mg mL^{-1}. Further increase in the MWCNT concentration results in a slight decrease in the current response, which could possibly be related to the increased thickness of the MWCNT film. Accordingly, 1.0 mg mL^{-1} of MWCNTs was selected for the preparation of the working electrode.

The amount of enzyme loaded on the electrode is also a crucial factor for the fabrication of the biosensor. Figure 4b shows the performance of the biosensor obtained as a function of the concentration of the immobilized uricase. The response current increases with the loaded uricase increasing from 0.2 to 1.0 mg mL^{-1}, indicating that the increase of the active site of enzyme at the electrode surface results in improved response sensitivity. However, too high the uricase concentration leads to a downward trend for the current response. It suggested that an excessively thick layer of enzyme film would block the diffusion of electrons from UA to the electrode. Therefore, an optimized enzyme concentration of 1.0 mg mL^{-1} was used to obtain the best response sensitivity.

Fixing the MWCNTs and the uricase concentration of 1.0 mg mL^{-1}, we further studied the effect of the applied potential in the range of 0.2–0.6 V on the performance of the biosensor. As illustrated in Fig. 4c, the current response of 100 μM UA increases with increasing the applied potential, up until 0.4 V. With the further increase in the applied

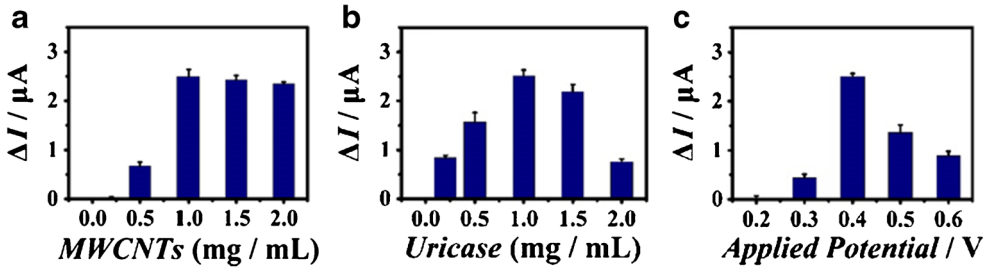

Fig. 4 Effect of **a** concentration of MWCNTs, **b** concentration of uricase, and **c** the applied potential on the current response of 100 μM UA at the biosensor

potential, however, the current response decreases. Therefore, the working potential was set at 0.4 V for the following chronoamperometry study.

Electrochemical evaluation of the biosensor in artificial saliva

The analytical performances of the biosensor were firstly evaluated in artificial saliva using chronoamperometric measurement under the optimized conditions. According to the average pH of healthy human saliva, the pH of artificial saliva was adjusted to 6.8 [29]. As shown in Fig. 5A, the enzyme catalytic reaction between the immobilized uricase and UA on the electrode surface results in a distinct signal change at the biosensor. The current response of the biosensor increases linearly with increasing the concentration of UA ranging from 5 to 1000 μM (Fig. 5B). The linear regression equation is expressed as $I\ (\mu A) = -0.011c\ (\mu M) - 1.532\ (R^2 = 0.993)$. The detection limit, evaluated using a signal-to-noise ratio of 3, is found to be 0.33 μM. The analytical performances for UA detection of the present method are compared with those obtained by other reported electrochemical biosensors, and the major parameters are summarized in Table 1. It can be seen that the method exhibits a relatively lower detection limit and a wider linear range which covers the full range of UA levels present in human saliva.

Selectivity is an important parameter for the biosensor since common co-existing physiological electroactive species, such as glucose, AA, and DA, can cause interference with the amperometric response of UA. Thus, prior to the application of the biosensor to human saliva samples, effect of common interfering species on the UA measurement was investigated. Figure 5C shows the chronoamperometric curve of the biosensor upon addition of UA, glucose, AA, DA, and a second UA, successively. It could be seen that the presence of glucose and DA did not interfere the detection of UA so much under the working potential. However, the addition of AA with 10 mM resulted in obvious current response. It should be noted that in authentic human saliva, these interferences are present at very low concentrations. The level of AA is normally about 1.4 μM in saliva [38], which is much lower than the concentration we chose to investigate here. Consequently, these potential interferences in real samples would have negligible influence on UA detection in saliva.

The electrode-to-electrode reproducibility was investigated by determining 100 μM UA using seven electrodes prepared independently by the same protocol (Fig. 5D). Chronoamperometry measurements for the seven detections yielded the RSD below 4.6% in the current response, confirming the good fabrication reproducibility of the biosensor. The stability of the biosensor was evaluated by storing it at 4 °C in buffer and measured intermittently. The amperometric response of the biosensor toward 100 μM UA still retained 90% of the initial value after 7 days of storage, suggesting a good stability of the biosensor.

Application of the biosensor in human saliva

The biosensor was then applied to determine UA in authentic human saliva samples using standard addition method. The typical amperometric responses of the biosensor for increasing the UA concentrations at 0.4 V are shown in Fig. 6A. For the

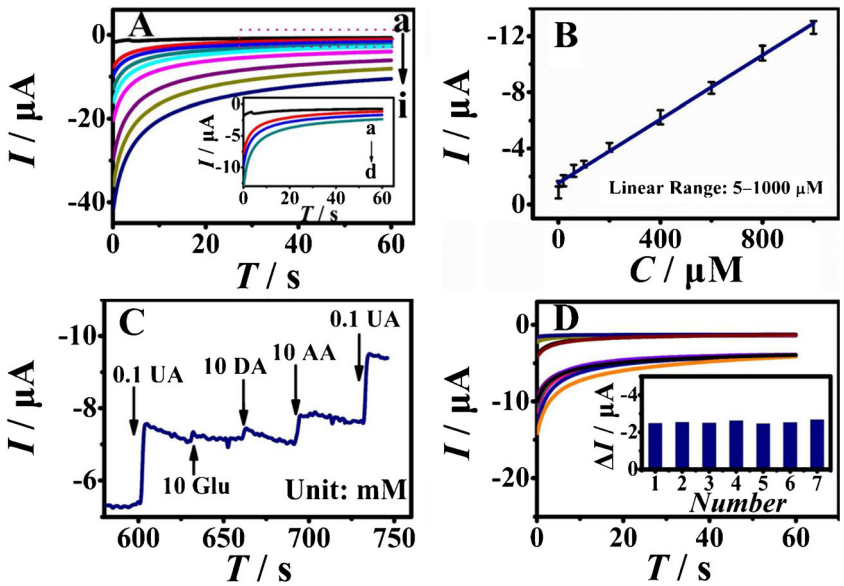

Fig. 5 **A** Chronoamperograms of the biosensor in artificial saliva containing different concentrations of UA (a–f: 5–1000 μM). Inset: the magnification of curves a–d. **B** The linear relationship between the current response and UA concentration. **C** Interference test recorded with the biosensor in artificial saliva. **D** Reproducibility study performed with seven biosensors for 100 μM UA

Table 1 Comparison of the performance of the biosensor with other biosensors

Electrode	Sample	Linear range (μM)	LOD (μM)	References
CS/uricase–PTBA–Pt_{nano}/Pt_{plate}/Au	Serum	5–1200	1	[30]
Uricase/CNT–CMC/Au	Serum	20–2700	2.8	[31]
Uricase/SPE–PB	Serum	30–300	10	[32]
Uricase/Au–rGO/ITO	Serum	50–800	7.32	[33]
GNP/uricase/Au	Serum	20–2500	7	[34]
Uricase–Th–SWNTs/GC	Serum	2–2000	0.5	[35]
Uricase/EDC:NHS/CZTS/ITO	--	0–700	0.66	[36]
Uricase/4–ASA/PB-GCE	Urine	10–200	3	[37]
Uricase/MWCNTs/SPE	Saliva	5–1000	0.33	This work

CS, chitosan; *PTBA*: poly(thiophene-3-boronic acid); *CMC*, carboxymethylcellulose; *PB*, Prussian blue; *GNP*, gold nanoparticles; *Th*, thionine; *EDC*, *N*-(3-dimethylaminopropyl)-*N*′-ethyl carbodiimide hydrochloride; *NHS*, *N*-hydroxysuccinimide; *CZTS*, Cu_2ZnSnS_4; *4–ASA*, poly(4–aminosalicylic acid)

saliva sample, a well-defined amperometric response baseline was firstly obtained owing to the uricase catalytic reaction between the immobilized uricase and UA in the sample (Fig. 6A, curve a). The consecutive additions of UA with designed concentrations to the saliva sample give linear responses of the current change as a function of concentrations (Fig. 6A, curves b to f). The linear relationship between the net steady sensing current and the UA concentration is I (μA) = −0.0072c (μM) − 1.28 (R^2 = 0.995) (Fig. 6B). The concentration of UA in the saliva sample was calculated according to the intercept of the calibration plot when the current is zero. The salivary UA in the given sample was found to be 176 μM, which is consistent with the previous reports [39, 40].

To explore the possible applications of the biosensor in clinical diagnosis, we next focus on the determination of salivary UA from hyperuricemia patients. Similar to the above results, based on the saliva baseline response, regularly increased chronoamperometry curves are achieved upon each increment of UA concentrations (Fig. 6C, curves b to f). There is a well-plotting linear relationship between UA concentration and the corresponding current signal. The linear equation is I (μA) = −0.0070c (μM)–3.29 (R^2 = 0.998) (Fig. 6D). From the calibration plot, the concentration of UA in the sample is estimated to be 470 μM. It can be seen that the salivary UA level of the hyperuricemia patient is significantly higher than that of the healthy volunteer. We further carried out the clinical analysis of the same sample using the uricase–peroxidase method at the wavelength of 520 nm to verify the accuracy of the developed method. According to the calibration plot of absorbance values of standard UA solution, the detected UA in the saliva sample from the

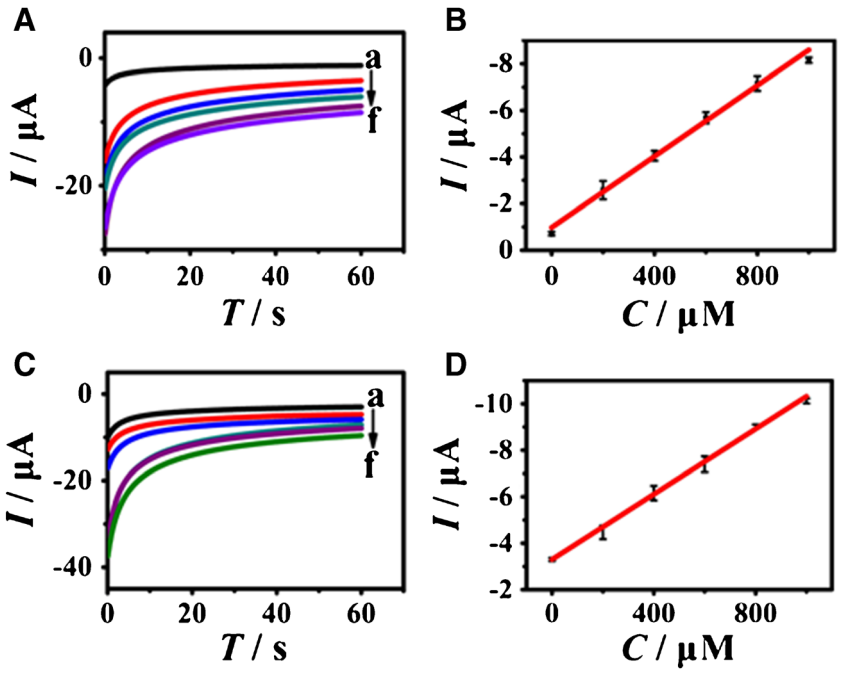

Fig. 6 Chronoamperometric response of saliva sample from a **A** healthy volunteer and **C** hyperuricemia patient spiked with increasing concentrations of UA in 200 μM increments (a–f). The resulting calibration plot from the **B** healthy volunteer and **D** hyperuricemia patient

hyperuricemia patient was 495 μM, which is consistent with the result of our current method. The consistency firmly confirmed the reliability and feasibility of the biosensor for assessing salivary UA in clinical applications. In addition, it is worth mentioning that in our method, the total time for single measurement was only 2 min and the required sample volume decreased to 100 μL, which is attractive for its practical application in point-of-care testing.

Conclusions

This work reports an uricase-based UA biosensor and its application in the salivary UA detection in authentic human saliva. The electrode modified with uricase on MWCNTs displayed favorable electrocatalytic capability toward UA with high sensitivity and selectivity, low detection limit, and wide linear range. The use of PET as substrate for fabrication of the biosensor featured with portability, low cost, flexibility, and disposability, which would be valuable in bioanalysis. More importantly, the salivary UA from the hyperuricemia patient without pretreatment was analyzed with the biosensor with results in accordance with the clinical test. This work demonstrates an easy and non-invasive method for salivary UA determination, which might open more opportunities for health care monitoring in clinical applications.

Funding information This work was financially supported by the National Natural Science Foundation of China (31741051, 21874077), Key R&D Projects of Jiangsu Province (BE 2019690), the Basic Science Research Program of Nantong City (JC2018066), the Science and Technology of R&D fund of Nantong City (XG202008-02), Qing Lan Project of Jiangsu Province, and the Jiangsu Overseas Visiting Scholar Program for University Prominent Young and Middle-Aged Teachers and Presidents.

Compliance with ethical standards

Conflict of interest The authors declare that they have no conflicts of interest.

Research involving human participants and/or animals All procedures performed in studies involving human participants were in accordance with the ethical standards of the institutional and/or national research committee and with the 1964 Helsinki declaration and its later amendments or comparable ethical standards. The collection of samples was approved by the Ethics Committee of the Affiliated Hospital of Nantong University, and the experiments on human biologic samples were approved by the Ethics Committee of Nantong University.

Informed consent Informed consent was obtained from all individual participants included in the study.

References

1. Marshall WJ. Clinical chemistry. 4th ed. Missouri: MOSBY; 2000.
2. Liao CZ, Mak C, Zhang M, Chan HLW, Yan F. Flexible organic electrochemical transistors for highly selective enzyme biosensors and used for saliva testing. Adv Mater. 2015;27:676–81.
3. Puig JG, Torres RJ, De Miguel E, Sánchez A, Bailén R, Banegas JR. Uric acid excretion in healthy subjects: a nomogram to assess the mechanisms underlying purine metabolic disorders. Metabolism. 2012;61:512–8.
4. Zoppini G, Targher G, Chonhol M, Ortalda V, Abaterusso C, Pivhiri I, et al. Serum uric acid levels and incident chronic kidney disease in patients with type 2 diabetes and preserved kidney function. Diabetes Care. 2012;35:99–104.
5. Sharaf El Din UAA, Salem MM, Abdulazim DO. Uric acid in the pathogenesis of metabolic, renal, and cardiovascular diseases: a review. J Adv Res. 2017;8:537–48.
6. Bel'skaya LV, Sarf EA, Kosenok VK. Age and gender characteristics of the biochemical composition of saliva: correlations with the composition of blood plasma. J Oral Biol Craniofac Res. 2020;10:59–65.
7. Hamzah HH. Spectrophotometric determination of uric acid in urine based–enzymatic method uricase with 4–aminodiphenylamine diazonium sulfate (Variamine Blue RT Salt). J Anal Bioanal Tech. 2013;S7:011.
8. Yue GZ, Li SY, Liu W, Ding F, Zou P, Wang XX, et al. Ratiometric fluorescence based on silver clusters and N, Fe doped carbon dots for determination of H_2O_2 and UA: N, Fe doped carbon dots as mimetic peroxidase. Sensors Actuators B Chem. 2019;287:408–15.
9. Ezoddin M, Adlnasab L, Afshari KA, Karimi MA. Ultrasonically formation of supramolecular based ultrasound energy assisted solidification of floating organic drop microextraction for preconcentration of methadone in human plasma and saliva samples prior to gas chromatography–mass spectrometry. Ultrason Sonochem. 2019;50:182–7.
10. Westley C, Xu Y, Thilaganathan B, Carnell AJ, Turner NJ, Goodacre R. Absolute quantification of uric acid in human urine using surface enhanced Raman scattering with the standard addition method. Anal Chem. 2017;89:2472–7.
11. Pang X, Li FS, Huang SQ, Yang ZQ, Mo Q, Huang L, et al. Electrostatically mediated layer–by–layer assembly of nitrogen–doped graphene/PDDA/gold nanoparticle composites for electrochemical detection of uric acid. Anal Bioanal Chem. 2020;412:669–80.
12. Wang YY, Liu X, Lu ZW, Liu T, Zhao LJ, Ding F, et al. Molecularly imprinted polydopamine modified with nickel nanoparticles wrapped with carbon: fabrication, characterization and electrochemical detection of uric acid. Microchim Acta. 2019;186:414.
13. Shi YT, Wang J, Li SM, Yan B, Xu H, Zhang K, et al. The enhanced photo–electrochemical detection of uric acid on Au nanoparticles modified glassy carbon electrode. Nanoscale Res Lett. 2017;12:455.
14. Huang HP, Yue YF, Chen ZZ, Chen YA, Wu SZ, Liao JS, et al. Electrochemical sensor based on a nanocomposite prepared from $TmPO_4$ and graphene oxide for simultaneous voltammetric detection of ascorbic acid, dopamine and uric acid. Microchim Acta. 2019;186:189.
15. Guan WH, Duan XX, Reed MA. Highly specific and sensitive non–enzymatic determination of uric acid in serum and urine by extended gate field effect transistor sensors. Biosens Bioelectron. 2014;51:225–31.
16. Cinti S, Talarico D, Palleschi G, Moscone D, Arduini F. Novel reagentless paper–based screen–printed electrochemical sensor to detect phosphate. Anal Chim Acta. 2016;919:78–84.
17. Barton J, García MBG, Santos DH, Fanjul-Bolado P, Ribotti A, McCaul M, et al. Screen–printed electrodes for environmental monitoring of heavy metal ions: a review. Microchim Acta. 2016;183:503–17.
18. Arduini F, Micheli L, Moscone D, Palleschi G, Piermarini S, Ricci F, et al. Electrochemical biosensors based on nanomodified screen–

printed electrodes: recent applications in clinical analysis. TrAC – Trends Anal Chem. 2016;79:114–26.
19. Cinti S, Arduini F. Graphene–based screen–printed electrochemical (bio)sensors and their applications: efforts and criticisms. Biosens Bioelectron. 2017;89:107–22.
20. Abellán-Llobregat A, Jeerapan I, Bandodkar A, Vidal L, Canals A, Wang J, et al. A stretchable and screen–printed electrochemical sensor for glucose determination in human perspiration. Biosens Bioelectron. 2017;91:885–91.
21. Jia LC, Li YK, Yan DX. Flexible and efficient electromagnetic interference shielding materials from ground tire rubber. Carbon. 2017;121:267–73.
22. Wen L, Li F, Cheng HM. Carbon nanotubes and graphene for flexible electrochemical energy storage: from materials to devices. Adv Mater. 2016;28:4306–37.
23. Liu YZ, Li GR, Guo Y, Ying YL, Peng XS. Flexible and binder–free bierarchical porous carbon film for supercapacitor electrodes derived from MOFs/CNT. ACS Appl Mater Interfaces. 2017;9:14043–50.
24. Navazesh M. Methods for collecting saliva. Ann N Y Acad Sci 1993.
25. Li SQ, Lin PF, Zhao LP, Wang C, Liu DY, Liu FM, et al. The room temperature gas sensor based on Polyaniline@flower–like WO_3 nanocomposites and flexible PET substrate for NH_3 detection. Sensors Actuators B Chem. 2018;259:505–13.
26. Kumar L, Rawal I, Kaur A, Annapoorni S. Flexible room temperature ammonia sensor based on polyaniline. Sensors Actuators B Chem. 2017;240:408–16.
27. Yaqoob U, Uddin ASMI, Chung GS. A high–performance flexible NO_2 sensor based on WO_3 NPs decorated on MWCNTs and RGO hybrids on PI/PET substrates. Sensors Actuators B Chem. 2016;224:738–46.
28. Gupta R, Singh B. Enhancement of electrical conductivity and magnetic properties of bimetallic Schiff base complex on grafting to MWCNTs. J Mater Sci Mater Electron. 2019;30:11888–906.
29. Bassoukou IH, Nicolau J, Santos MT. Saliva flow rate, buffer capacity, and pH of autistic individuals. Clin Oral Investig. 2009;13:23–7.
30. Huang Y, Bu LJ, Wang W, Qin XL, Li Z, Huang Z, et al. One–pot preparation of uricase–poly(thiophene–3–boronic acid)–Pt nano composites for high–performance amperometric biosensing of uric acid. Sensors Actuators B Chem. 2013;177:116–23.
31. Fukuda T, Muguruma H, Iwasa H, Tanaka T, Hiratsuka A, Shimizu T, et al. Electrochemical determination of uric acid in urine and serum with uricase/carbon nanotube/carboxymethylcellulose electrode. Anal Biochem. 2020;590:113533.
32. Piermarini S, Migliorelli D, Volpe G, Massoud R, Pierantozzi A, Cortese C, et al. Uricase biosensor based on a screen–printed electrode modified with Prussian blue for detection of uric acid in human blood serum. Sensors Actuators B Chem. 2013;179:170–4.
33. Verma S, Choudhary J, Singh KP, Chandra P, Singh SP. Uricase grafted nanoconducting matrix based electrochemical biosensor for ultrafast uric acid detection in human serum samples. Int J Biol Macromol. 2019;130:333–41.
34. Liu Y, Yuan M, Liu LL, Guo R. A facile electrochemical uricase biosensor designed from gold/amino acid nanocomposites. Sensors Actuators B Chem. 2013;176:592–7.
35. Chen D, Wang Q, Jin J, Wu P, Wang H, Yu S, et al. Low–potential detection of endogenous and physiological uric acid at uricase–thioninesingle–walled carbon nanotube modified electrodes. Anal Chem. 2010;82:2448–55.
36. Jain S, Verma S, Singh SP, Sharma SN. An electrochemical biosensor based on novel butylamine capped CZTS nanoparticles immobilized by uricase for uric acid detection. Biosens Bioelectron. 2019;127:135–41.
37. da Cruz FS, Paula F d S, Franco DL, dos Santos WTP, Ferreira LF. Electrochemical detection of uric acid using graphite screen–printed electrodes modified with Prussian blue/poly(4–aminosalicylic acid)/uricase. J Electroanal Chem. 2017;806:172–9.
38. Shetty SR, Babu S, Kumari S, Prasad R, Bhat S, Fazil KA. Salivary ascorbic acid levels in betel quid chewers: a biochemical study. South Asian J Cancer. 2013;2:142–4.
39. Shibasaki K, Kimura M, Ikarashi R, Yamaguchi A, Watanabe T. Uric acid concentration in saliva and its changes with the patients receiving treatment for hyperuricemia. Metabolomics. 2012;8:484–91.
40. Ngamchuea K, Batchelor-McAuley C, Compton RG. Understanding electroanalytical measurements in authentic human saliva leading to the detection of salivary uric acid. Sensors Actuators, B Chem. 2018;262:404–10.